Integrating Voltammetry and Substrate-Enhanced Luminescence for Noninvasive Glucose Sensing

Gabriel López-Peña[a], Ana Pallarés Vilar[a,b], Aida Jaafar[c], Silvia Simón-Fuente[c] , Antonio Arranz[a], Maria Ribagorda[c,e], Miguel Manso-Silván[a,d,f], Emma Martín Rodríguez[a,d,e,g]

[a] Departamento de Física Aplicada, Universidad Autónoma de Madrid, C/ Francisco Tomás y Valiente 7, 28049, Madrid, Spain.
[b] Departamento de Química en Ciencias Farmacéuticas, Universidad Complutense de Madrid, 28040, Madrid, Spain.
[c] Departamento de Química Orgánica, Universidad Autónoma de Madrid, C/ Francisco Tomás y Valiente 7, 28049, Madrid, Spain.
[d] Instituto de Ciencia de Materiales Nicolás Cabrera, Universidad Autónoma de Madrid, C/ Francisco Tomás y Valiente 7, 28049, Madrid, Spain.
[e] Institute for Advanced Research in Chemical Sciences (IAdChem), Universidad Autónoma de Madrid, C/ Francisco Tomás y Valiente 7, 28049, Madrid, Spain
[f] Centro de Micro-Análisis de Materiales, Universidad Autónoma de Madrid, C/ Francisco Tomás y Valiente 7, 28049, Madrid, Spain.
[g] Nanomaterials for BioImaging Group, Instituto Ramón y Cajal de Investigación Sanitaria IRYCIS, Ctra. de Colmenar km 9,300, 28034, Madrid, Spain.

* Corresponding author's e-mail address: emma.martin@uam.es

Abstract

This study presents a novel noninvasive and enzyme-free dual sensor based on porous silicon for the detection of D-glucose through tear fluid analysis. The sensor incorporates $NaGdF_4$:20% Yb^{3+}, 2% Er^{3+} nanoparticles (YbEr-NPs) immobilized on a porous silicon substrate functionalized with a phenylboronic ester molecule. The YbEr-NPs enable luminescence-based sensing, exploiting the sensitivity of Er^{3+} ions to the OH vibrational groups present in D-glucose. Electrodes fabricated on a porous silicon substrate allow for voltammetric analysis, providing a second detection method. The voltammetric sensor achieved a limit of detection (LoD) of 20 mg/dL in the range of 20-200 mg/dL, which is suitable for detecting D-glucose concentrations in the tear fluid of diabetic patients. The luminescence-based sensor, utilizing the red-to-green emission ratio of YbEr-NPs, reached a LoD of 140 mg/dL in the range of 10-70 mg/dL, covering the hyperglycemic range. The interaction between the YbEr-NPs and the porous silicon substrate led to the appearance of new emission bands and increased intensity, attributed to surface defects acting as an additional excitation source. The 556 nm emission band showed a strong dependence on the D-glucose concentration, improving the LoD to 110 mg/dL. This provides a novel strategy for D-glucose detection based on the effect of the molecule on the interaction between the UCNPs and the Psi substrate. This triple-sensing approach offers a promising solution for noninvasive glucose monitoring, enabling detection in both the hypoglycemic and hyperglycemic ranges.

Keywords: porous silicon, glucose sensor, D-glucose, rare earths, nanoparticles

1. Introduction

In 2021, the International Diabetes Federation (IDF) estimated that diabetes mellitus affected 537 million people worldwide and predicted that this number will increase to 783 million by 2045 [1]. Patients with this disease present with a chronic metabolic disorder characterized by high blood glucose levels resulting from insufficient insulin production or ineffective insulin utilization by the body. Healthy blood glucose levels are usually between 70 and 100 mg/dL, whereas hypoglycemia can occur when these levels drop below 70 mg/dL. In contrast, high blood glucose levels are usually > 125 mg/dL [2–8]. Therefore, in most cases, patients are required to monitor their blood glucose levels several times a day, involving piercing their fingers or forearms to collect small amounts of blood in most cases [9]. This method can be considered invasive because it causes discomfort to patients or the appearance of calluses in pierced areas. Moreover, this method consumes large amounts of supply [9,10].

Optical coherence tomography [11–13], surface plasmon resonance [14–16], Raman spectroscopy [17–20], photoacoustic analysis [21], and fluorescence measurements [22–24] are noninvasive methods developed to avoid the extraction of blood from patients, which is usually achieved by analyzing other physiological fluids, such as saliva [25–27], sweat [28–30], urine [31,32], interstitial fluid [33–35], and tear fluid [8,36–39]. In particular, tear fluid provides direct information about blood glucose levels in patients, as tears are formed in the lacrimal glands, which are generated through filtration from the plasma after circulation throughout the body. Most proteins in the plasma can be found in the tear fluid, and some are related to albumin, urea, cholesterol, and glucose [40,41]. All the information that the analysis of tear fluid can provide has opened the path for understanding diseases such as Parkinson's, Alzheimer's, cystic fibrosis, cancer, sclerosis, and diabetes mellitus [42–45]. However, one of the main limitations of tear fluid in the field of glucose level control is that it presents much lower concentrations than those found in the blood. To solve this problem, the development of sensing probes with high sensitivity and specificity is one of the main goals for achieving efficient noninvasive glucose sensing.

Rare-earth-doped nanoparticles (RENPs) have demonstrated exceptional capabilities as sensing probes. The excellent properties of these materials, such as narrow emission bands, which can be tuned by selecting different ions as dopants; their long lifetimes in the range of micro- or even milliseconds; their reduced photobleaching; and their ability to show changes in luminescence depending on different factors such as pH, pressure, temperature, or molecular environment, make them an excellent choice for sensing applications [46–49]. Among the different combinations of ions that can compose RENPS, Er^{3+} and Yb^{3+} ions are two of the most common in the sensing field, particularly for detecting temperature changes [50,51]. Additionally, Er^{3+} ions interact with the OH vibrational levels, altering the relative intensities of several Er^{3+} emission bands [52]. This enables D-glucose concentration measurement [39], eliminating the need for enzymes to enhance the sensor and avoiding enzyme-related stability issues [53,54]. Although there are RENPs-based sensors capable of indirectly measuring glucose concentrations (e.g., through the presence of H_2O_2 formed by the interaction between the glucose oxidase enzyme and a nanomaterial [55]), their number is reduced [56–59], and even more so in regard to sensors that directly measure the presence of glucose through fluorescence methods [39,60].

Another point of interest in the development of an effective sensor is the selection of the substrate, which can affect the performance, sensitivity, selectivity, and stability of the sensor. In this work, we chose porous silicon as the sensor substrate because it has been

widely used in biological applications owing to its outstanding properties, such as its high specific surface area (which allows increasing the number of sensing probes on the sensor surface), biocompatibility, ease of functionalization, ability to control the pore diameter by simply changing the fabrication parameters, low cost of the material, and compatibility with the majority of devices in the semiconductor industry [61–63]. Moreover, the selection of this rigid material as a substrate provided a stable surface for the immobilization of YbEr-NPs, which also increased the stability and precision of the device. Additionally, porous silicon is a widely used material for sensor fabrication because electrodes can be easily included on its surface to enable electrochemical sensing, offering the possibility of a dual sensing mechanism when combined with NPs [64].

We have developed a dual porous silicon-based sensor with RENPs containing Er^{3+} and Yb^{3+} ions acting as sensing probes, contributing to the current state of the art in the noninvasive glucose sensing field. The novelty of this work lies not only in the use of RENPs for the direct enzyme-free and fluorescence-based detection of D-glucose but also in the possibility of dual sensing, harnessing the potential of voltammetric analysis owing to the electrodes of the sensor, and fluorescence analysis due to the use of RENPs.

2. Materials and methods

2.1. Synthesis of $NaGdF_4$:20% Yb^{3+}, 2% Er^{3+}.

$NaGdF_4$:20% Yb^{3+}, 2% Er^{3+} nanoparticles were synthesized using a standard thermal decomposition method. A mixture containing 2.5 mmol of $GdCl_3$, $YbCl_3$, and $ErCl_3$, 25 mL of octadecene, and 25 mL of oleic acid was heated to 120 °C under vacuum for 1 h, followed by the addition of 0.85 g of sodium trifluoroacetate. Subsequently, the temperature was increased to 300 °C for 2 h.

2.2. Synthesis of alkoxysilane boronic ester molecules.

4-Aminophenylboronic acid pinacol ester (250 mg, 1.1 mmol, 1.0 equiv.) was added to a microwave-sealed tube equipped with a stirring bar. The tube was evacuated and flushed with argon three times before 4.6 mL of dry THF (0.2 M) were added. Subsequently, 3-(triethoxysilyl)propyl isocyanate (0.3 mL, 1.1 mmol, 1.0 equiv.) was added dropwise. The reaction mixture was then stirred at 70 °C for 16 h. The solvent was removed under reduced pressure, and the residue was purified by flash column chromatography using heptane:ethyl acetate (4:1) as the eluent to afford the desired product as a white powder (315 mg, 62% yield). A schematic of the synthetic process is shown in **Figure S1**. **^{1}H NMR** (300 MHz, $CDCl_3$): δ = 7.4 (d, *J* = 8.5 Hz, 2H), 7.3 (d, *J* = 8.5 Hz, 2H), 6.45 (s, 1H), 5.0 (t, *J* = 5.8 Hz, 1H), 3.8 (q, *J* = 7.0 Hz, 6H), 3.25 (td, *J* = 7.0, 5.8 Hz, 2H), 1.67 (m, 2H), 1.3 (s, 12H), 1.2 (t, *J* = 7.0 Hz, 9H), 0.65 (t, *J* = 8.2 Hz, 2H). ^{13}C NMR (125 MHz, $CDCl_3$): δ = 156.17, 142.15, 135.96, 118.54, 83.64, 58.53, 42.70, 24.90, 23.56, 18.33, 7.61. HRMS: Calc. for $C_{22}H_{39}BN_2O_6Si$ (M+): 466.3 found: 467.3. M.p.: 86.2 °C

2.2. Porous silicon preparation

The silicon wafers used for the preparation of PSi had a thickness of 500 µm and a resistivity of 0.02 − 0.021 Ωcm, with a <100> crystal orientation. From these wafers, 1.5 cm^2 fragments were obtained using a diamond cutter. Once the silicon wafers were prepared, their surfaces were cleaned with ethanol to remove any impurities and then placed in an electrochemical etching cell. The wafers were then introduced into a

mixture of hydrofluoric acid (HF, 48%) and absolute ethanol in a 1:2 ratio. With the wires positioned correctly, a current of 98.2 mA was applied for 30 s. The current and time parameters were selected based on previous studies conducted by a research group [65–67].

2.3. Arylboronic ester functionalised-PSi

A drop containing 20 µL of *p*-(triethoxysilyl)alkyl-phenyl boronic ester (10 mg/mL in ethanol) was added to the PSi wafer. After addition, the wafer was left to dry for 5 min, after which the final drying process was performed using a nitrogen gun.

2.4. Electrode fabrication

The slots for the electrodes were fabricated by cleaning the silicon surface using an ion gun operating at 800 V for 20 min. A mask carved in silicon with the desired electrode shape was used to create the slots. Subsequently, a 20 min sputtering process with a nickel-chrome alloy disk was performed to create the first layer of the electrodes. Finally, a second 2 min sputtering process with gold was performed to finish the electrodes and improve their conduction properties.

2.5. Transmission electron microscopy.

Transmission electron microscopy (TEM) images were obtained using a JEOL JEM1010 microscope (JEOL) operating at 100 kV. The samples were prepared by dropping sample dispersions (0.1 - 0.5 mg/mL in hexane) onto a 300-mesh carbon-coated copper grid (3 mL in diameter) followed by evaporation of the solvent.

2.6. Scanning electron microscopy.

Morphological characterization of the porous silicon (PSi) wafers was carried out using a field-emission scanning electron microscope (FESEM; Philips XL-40FEG) and a conventional SEM (Philips XL30), both operated at 20 keV.

2.7. Fourier-transform infrared spectroscopy

The Fourier transform infrared (FTIR) spectra presented in this work were measured with an ATR-FTIR module of the Cary 630 FTIR (Agilent) by depositing a droplet of the desired dispersion on a diamond cell and allowing the solvent to evaporate.

2.8. X-ray photoelectron spectroscopy (XPS)

The XPS experiments performed in this study were carried out at the Institute of Catalysis and Petrochemistry (CSIC, Universidad Autónoma de Madrid Campus) in an ultra-high vacuum chamber using a SPECS GmbH system with a PHOIBOS 150 9MCD analyzer and a non-monochromatic Al-Kα X-ray source fed at a constant power of 100 W. For the analysis of the XPS spectra, the binding energies (BE) were determined by referencing the C1s peak of the C-C species at 285 eV.

2.9. Contact angle.

Contact angle measurements were performed using an optical contact angle and surface tension meter (CAM 101, KSV Instruments Ltd.), where a needle allowed the deposition of a drop of water (or any other liquid if desired) onto the surface of the analyzed material. The equipment included a camera to acquire images of the drop surface. The

analysis of these images was performed using the KSV Contact Angle Measurement System software.

2.10. Cyclic voltammetry

Cyclic voltammetry measurements were carried out using a BioLogic SP-150 voltammetry equipment, which allowed cyclic voltammetry measurements to be performed over a voltage range from −1.5 to 1.5 V at a scan rate of 20 mV/s.

2.11. Up-conversion emission spectra

To collect the up-conversion emission spectra, a homemade collection system composed of an 800 nm diode laser, several mirrors, and lenses was used. An iHR320 HORIBA monochromator and a cooled CCD array Synapse HORIBA detector were used to collect the spectra.

3. Results and discussion

3.1. Fabrication and characterization of the PSi-based sensor.

$NaGdF_4$:20% Yb^{3+}, 2% Er^{3+} nanoparticles (YbEr-NPs) were synthesized using a thermal decomposition method. The TEM images of the synthesized YbEr-NPs showed a non-aggregated distribution (**Figure S2A**), and further statistical analysis showed that the YbEr-NPs had a mean diameter of 32 ± 11 nm (**Figure S2B**). The energy level diagram of the YbEr-NPs (**Figure 1A**) shows that the energy of 980 nm photons absorbed by Yb^{3+} ions can be transferred to the Er^{3+} ions through a two-step Yb^{3+} " Er^{3+} energy transfer, thus populating the $^4F_{7/2}$ energy level of Er^{3+} ions, a process known as upconversion. This generated the main visible emissions of the YbEr-NPs in the green (500 – 580 nm) and red (620 – 700 nm) regions from the $^2H_{11/2}$:$^4S_{3/2}$ and $^4F_{9/2}$ energy levels, respectively (**Figure 1B**). Under normal conditions, crossing the energy gap from the $^2H_{11/2}$/$^4S_{3/2}$ levels to the $^4F_{9/2}$ level requires approximately nine lattice phonons (the phonon energy of the $NaGdF_4$ lattice is 350 cm^{-1}), leading to a higher probability (and thus higher intensities) of green emissions than red ones. However, when Er^{3+} ions are in the presence of OH vibrational groups, the OHs can act as efficient energy bridges that transfer the population from the $^2H_{11/2}$:$^4S_{3/2}$ levels to the $^4F_{9/2}$ level, increasing the probability of red emission.[52] This demonstrated sensitivity towards OH vibrational groups, one of the main components of the D-glucose molecule, motivated the selection of Er^{3+} and Yb^{3+} as doping ions [52].

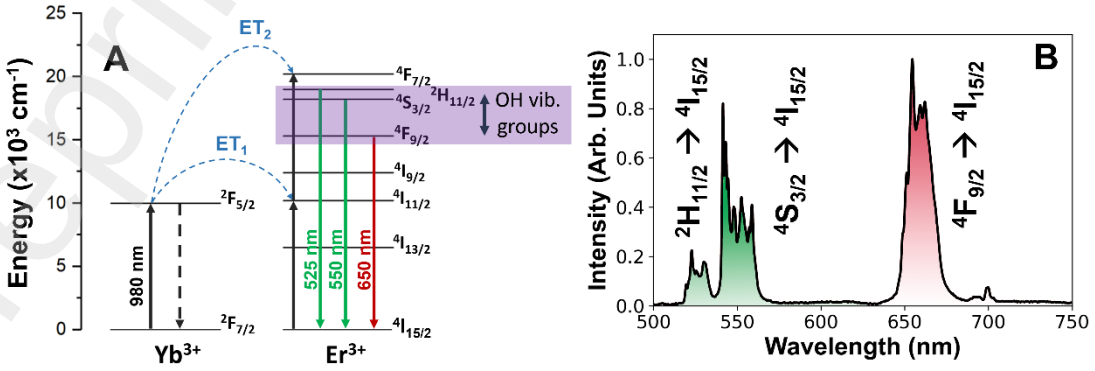

Figure 1. A. Energy level diagram of the rare earth ions composing the YbEr-NPs. **B.** Up-conversion emission of an aqueous dispersion (10 mg/mL) of YbEr-NPs under 980 nm diode laser excitation.

Porous silicon (PSi) was used as a substrate for the sensor. PSi has already been widely used in biological applications owing to its outstanding properties. PSi was prepared by the classical electrochemical etching method using a mixture of hydrofluoric acid and ethanol in a 1:2 proportion. The obtained PSi wafers presented an organized and homogeneous pore distribution on their surfaces with a mean pore size of 91 ± 11 nm (**Figure S3**), allowing not only the distribution of the YbEr-NPs on the surface but also inside the pores. However, before PSi can be used as a substrate, the material underwent a treatment to improve its hydrophilicity and obtain an even distribution of the analyzed sample on the surface of the sensor. For this purpose, the PSi wafers were submerged for 20 min in hydrogen peroxide (H_2O_2) to facilitate the oxidation of the superficial layer of the PSi wafer because SiO_2 is known to have a higher degree of hydrophilicity than non-oxidized PSi [68]. This procedure increased the hydrophilicity of the substrate, leading to a final contact angle of 4 ° (**Figure S4A**), which ensured the complete and even distribution of the analyte on the sensing surface. After this treatment, the PSi wafers were submerged for 40 s in a 10 mg/mL dispersion of oleate-free YbEr-NPs to integrate the NPs into the device.

One of the benefits of using YbEr-NPs as sensing probes is that we do not need the use of enzymes to increase selectivity towards glucose because the luminescence-based sensing mechanism is very sensitive to the presence of OH groups in the glucose molecule. Additionally, it is likely that glucose molecules bind to the surface of the YbEr-NPs. For this reason, XPS analysis was performed to obtain more information about the effect of adding D-glucose to the surface of the YbEr-NPs and the possibility of obtaining proof of new chemical bonds between the molecules and NPs. For this purpose, two samples were prepared: first, a PSi-SiO_2 wafer was covered with YbEr-NPs; second, a PSi-SiO_2 wafer was covered with YbEr-NPs and then with a layer of D-glucose. **Figure 2** shows the main results of the experiment. The upper part of the graphs (blue line) shows the analysis of the PSi-SiO_2 wafers covered with YbEr-NPs, and the lower part (red line) shows the analysis of the PSi-SiO_2 wafers covered with the above-mentioned YbEr-NPs and D-glucose. **Figure 2A** shows the C 1s core level, where it can be observed that the spectrum can be deconvoluted into three contributions associated with the C-C, C-O, and C=O chemical species. After the addition of D-glucose, the intensity of the component associated with the C-C bond increased due to the abundance of carbon in the D-glucose molecule. The Si 2p core level (**Figure 2B**) is composed of a SiO_2 component at higher binding energies and a Si component at lower binding energies. After the addition of D-glucose, the intensities of the SiO_2 and Si components decreased because the wafer was covered with the molecules, which reduced the signal collected from the substrate. **Figure 2C** shows that the spectrum of the Gd $3d_{5/2}$ core level of YbEr-NPs has a complex shape because of the multiplet-splitting effects characteristic of the Gd core levels in different compounds [69]. This core level did not undergo shape changes upon the addition of D-glucose, suggesting that no new chemical species of Gd appeared after the deposition of the molecule over the YbEr-NPs. Additionally, it should be expected that the intensity of the Gd $3d_{5/2}$ core level after the addition of D-glucose would decrease; instead, we observed an increase in the intensity. We attributed this behavior to the possibility of analyzing an area of the PSi-SiO_2 wafer with a higher concentration or accumulation of YbEr-NPs in the second XPS experiment, which led to an increase in the signal intensity. Finally, **Figure 2D** shows the Gd $4d_{5/2}$ and $4d_{3/2}$ core levels of the YbEr-NPs

and the Si 2s core level of the PSi-SiO_2 wafer. The Gd 4d core level also has a complex shape owing to multiplet-splitting effects, such that several peaks were necessary to reproduce the overall shape at this core level in previous studies [39]. We conclude that the changes observed in the Gd 4d core level after the addition of D-glucose may be attributed to the formation of a new chemical species related to the bonding between the NPs and D-glucose. However, in this study, it was more difficult to ascertain the changes in the Gd 4d core level upon the addition of D-glucose because of the high intensity of the Si 2s signal and the severe overlap of this signal with the Gd $4d_{3/2}$ core level observed in the spectrum of the PSi-SiO_2 wafer covered with YbEr-NPs before the addition of D-glucose. However, the slight increase in intensity observed in the low binding energy region of the Gd $4d_{5/2}$ region suggests some kind of interaction between the NPs and D-glucose.

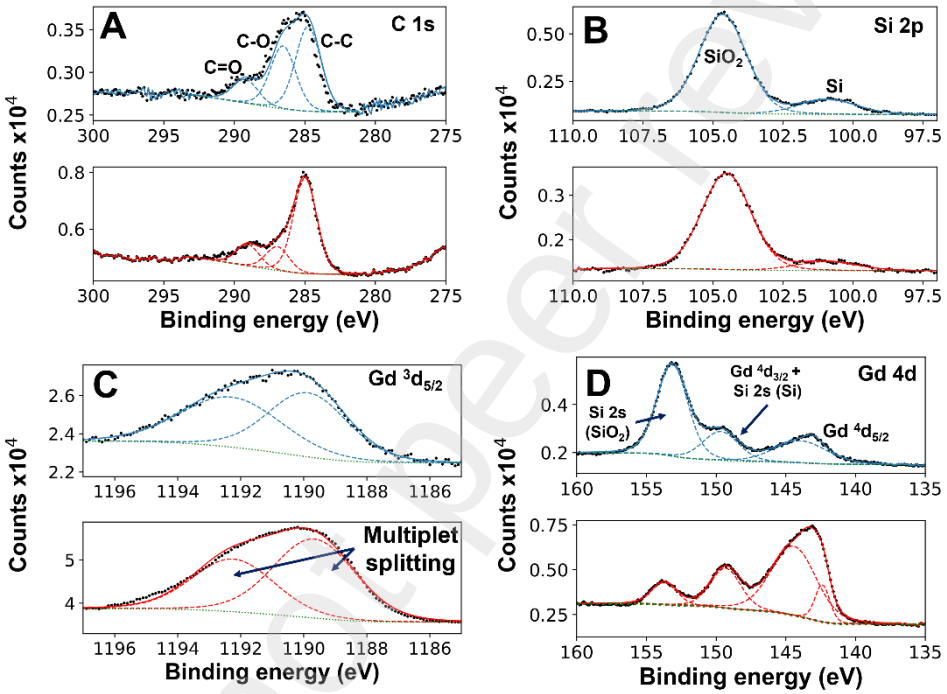

Figure 2. A. High-resolution XPS spectra analysis of the C 1s (**A**), Si 2p (**B**), Gd 3d5/2 (**C**) and Gd 4d (**D**) core levels. The blue lines in the upper graphs correspond to the samples with PSi-SiO_2 and YbEr-NPs, whereas the red lines in the lower graphs represent the samples with PSi-SiO_2, YbEr-NPs, and D-glucose. The dotted green line corresponds to the spectral background.

Although we demonstrated in previous studies that these types of nanoparticles are capable of detecting small changes in D-glucose concentrations without the need to enhance their sensing mechanism [39], we decided to increase the efficiency and specificity of our porous silicon-based sensor by adding an organic molecule containing a phenylboronic ester with a pendant *p*-(triethoxysilyl)alkyl group immobilized on the surface of the PSi wafer. The triethoxysilyl ending group serves to anchor the entire molecule to the SiO_2 layer of the PSi wafer, whereas the boronic ester end enables specificity towards D-glucose sensing (**Figure S4B**). Boronic acids and esters can react with 1,2- or 1,3-diols, which are hydroxyl (OH) chemical entities present in D-glucose molecules, creating a boronate ester through a reversible covalent linkage between OH and the boron atom [70]. Functionalized PSi was obtained by adding a 20 µL drop of *p*-(triethoxysilyl)alkyl-phenyl boronic ester (10 mg/mL in ethanol) to the PSi wafer. FTIR experiments were conducted to assess the presence of

boronic esters on the wafer surface (see **Figure S5** for details). Initially, no significant peaks were observed owing to superficial oxidation. However, after boronic ester addition, bands related to B-O and C=O vibrations appeared. Glucose was then added to two wafers: one with boronic ester and the other without boronic ester. Subsequent FTIR measurements revealed stronger peaks in the wafer with boronic ester, confirming its ability to enhance D-glucose fixation.

3.2. Voltammetric analysis

As mentioned, one of the novel aspects of our sensor is its ability to detect changes in the concentration of D-glucose using two different methods: luminescence and voltammetric analysis. The first method takes advantage of the presence of YbEr-NPs in the substrate and how their luminescence is affected by the presence of D-glucose, whereas the second method uses electrodes fabricated on top of the wafer to analyze the changes in the intensity-voltage curves for different concentrations of D-glucose. Voltammetric analysis was performed by positioning the PSi wafers in a homemade device with two conductive pins in contact with the electrodes. An increasing voltage of 0–5 V was applied to the electrodes (**Figure 3A**). The changes in intensity were recorded after several immersions in a solution of D-glucose in water, producing changes in the concentration from 0 to 200 mg/dL. The different intensity-voltage curves for the studied concentration ranges are shown in **Figure 3B**. The curve measured in the absence of D-glucose presented lower current values than those in the absence of D-glucose. These differences are consistent with the oxidation of D-glucose, leading to the formation of gluconolactone and thus to the release of protons in the electrodes, amplifying the current. From these data, a calibration curve relating the maximum measured intensity to the concentration of D-glucose was obtained (**Figure 3C**). From this curve, the limit of detection (*LoD*) of the voltammetric sensor was obtained as $LoD = 3\sigma/m$, where σ is the standard deviation of 10 consecutive measurements of a blank sensor (in the absence of D-glucose, **Figure 3D**), and m is the slope of the obtained calibration curve. A *LoD* of 20 mg/dL was achieved in the studied range between 20 and 200 mg/dL, which is an exceptional result for future applications of these sensors in noninvasive glucose sensing through tear fluid, as the usual concentration of D-glucose in tear fluid for diabetic patients can range from 0 to 84 mg/dL [8].

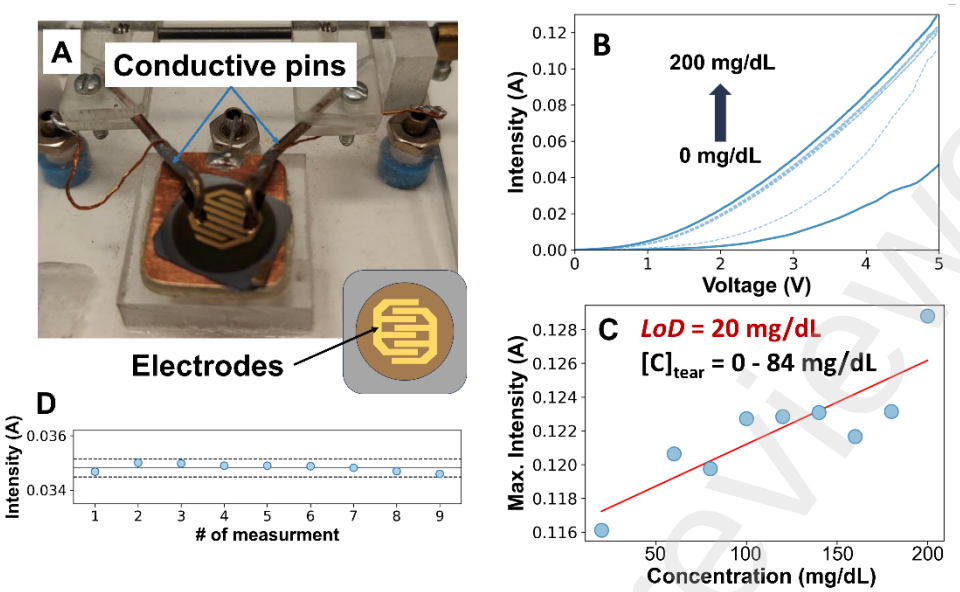

Figure 3. A. Image of the used setup for the voltammetric analysis. **B.** Intensity-voltage curves for the different concentrations of D-glucose ranging from 0 to 200 mg/dL for applied voltages between 0 and 5 V. **C.** Calibration curve representing the relationship between the maximum intensity measured at 5 V and the concentration of D-glucose. **D.** Consecutive measurements of the blank sensor used to calculate *LoD*. The upper and lower discontinuous lines represent the calculated standard deviations.

3.3. Luminescence analysis

Finally, it is necessary to explore the ability of our devices to sense changes in the concentration of D-glucose through the luminescence of YbEr-NPs. As mentioned previously, integration of the NPs into the PSi wafers was performed by immersing the wafers in a 10 mg/mL aqueous dispersion of oleate-free YbEr-NPs for 40 s. This method was optimized by analyzing the luminescence intensity of the NPs in the wafers after several immersions at different times. The maximum possible intensity was achieved after 40 s. The stability of the YbEr-NPs on the surface of the sensor was demonstrated by rinsing the wafers with abundant ethanol and measuring the emission intensity afterwards (**Figure S6**). The changes in the luminescence intensity were minimal after this process, indicating that the sensor presented no reversible character; however, because they were designed as a one-use sensor, this does not pose a drawback. Therefore, we conclude that future immersion of wafers in aqueous media does not affect the concentration of YbEr-NPs on the wafer.

PSi wafers containing YbEr-NPs were submerged in a solution of D-glucose in water (10 mg/dL) for 60 s. After the wafers were dried, their luminescence was measured. This process was repeated several times until a maximum D-glucose concentration of 70 mg/dL was reached. Interestingly, the obtained spectra (**Figure 4A**) showed that the emission intensity of the YbEr-NPs green emission band increased instead of decreasing with increasing D-glucose concentration. Moreover, no luminescence from the PSi substrate was observed, because UV light was not used to excite the YbEr-NPs, thus removing this method as a source of uncertainty in our measurements. A calibration curve relating this ratio to the D-glucose

concentration was obtained by measuring the red-to-green ratio of the different samples (**Figure 4B**). The LoD of the luminescence-based sensor was calculated from this calibration curve, and a value of 140 mg/dL was obtained in the studied range of 10–70 mg/dL.

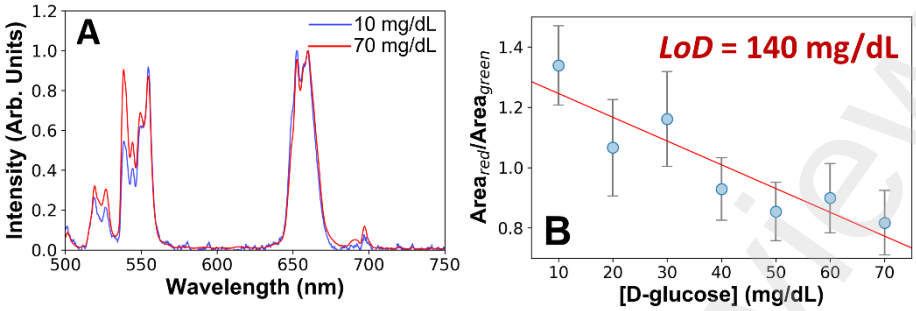

Figure 4. A. Comparison of the up-conversion emission of YbEr-NPs in the presence of the minimum (blue) and maximum (red) D-glucose concentrations used in this experiment. **B.** Calibration curve representing the relationship between the red-to-green ratio and D-glucose concentration.

As mentioned, the behavior of the up-conversion emission of the YbEr-NPs in the presence of D-glucose differs from theory because the intensity of the green band increases with the number of sugar molecules. To shed light on this result, the behavior of the YbEr-NPs in the PSi wafer was studied. Therefore, a more extended emission spectrum (from blue to green) was observed. **Figure 5A** shows a comparison between the spectra of YbEr-NPs in a water dispersion (10 mg/mL) and PSi wafers. The bands at 406 nm ($^2H_{9/2}$ " $^4I_{15/2}$), 467 nm ($^2P_{3/2}$ " $^4I_{11/2}$), and 501 nm ($^4F_{7/2}$ " $^4I_{15/2}$) showed an increase in the emission intensity when the YbEr-NPs were in the PSi substrates. Moreover, the green region is heavily affected, showing clear changes in the bands at approximately 525 nm ($^2H_{11/2}$ " $^4I_{15/2}$) and 556 nm ($^2H_{9/2}$ " $^4I_{13/2}$). In contrast, only a slight increase in the emission intensity of the red band at approximately 660 nm ($^2F_{9/2}$ " $^4I_{15/2}$) was observed (**Figure S7**). It is well known that the shape of the emission spectrum can change with increasing power density of the excitation laser [71,72]. We ruled out this possibility by comparing the shape of the emission spectrum of a 10 mg/mL aqueous dispersion of YbEr-NPs obtained with a power density of 4.5 mW/cm^2 (the same one used for the experiments presented here) with the spectrum obtained with a much higher power density (25 mW/cm^2). The increase in power density induced changes in the shape of the spectrum, but the power density did not reach the level of when YbEr-NPs were present in the PSi wafers (**Figure S8**).

From this point, it is clear that the increase in the emission intensity of some bands is related to the interaction between the YbEr-NPs and the PSi substrate. Moreover, it can be observed that some of the affected bands (406, 467, and 556 nm) involve the absorption of more than two photons by the system to reach superior levels. We tentatively explained this behavior through the presence of surface defects or surface states in PSi, which can lead to a population of higher energy levels of the Er^{3+} ions. These surface defects can act as energy wells, retaining energy from the excitation source and quickly releasing it again because they are very unstable [73,74]. This extra excitation source from the surface defects can lead to a

population with higher Er^{3+} energy levels, and thus, to the appearance of new emission bands and an increase in the emission intensity (**Figure 5B**). Interestingly, if high concentrations of D-glucose are added to the surface of the PSi wafers, it can be observed that the shape of the spectrum "recovers" the shape that the YbEr-NPs show when they are in an aqueous dispersion (**Figure 5C**). The addition of D-glucose to the surface of the sensor prevents surface defects from harvesting energy from the excitation source because D-glucose covers them. Moreover, it can be observed that the green emission band at 556 nm is strongly dependent on D-glucose. We calculated the ratio between the green emission bands at 556 and 540 nm and obtained a new and more sensitive calibration curve (**Figure 5D**) with an improved *LoD* of 110 mg/dL.

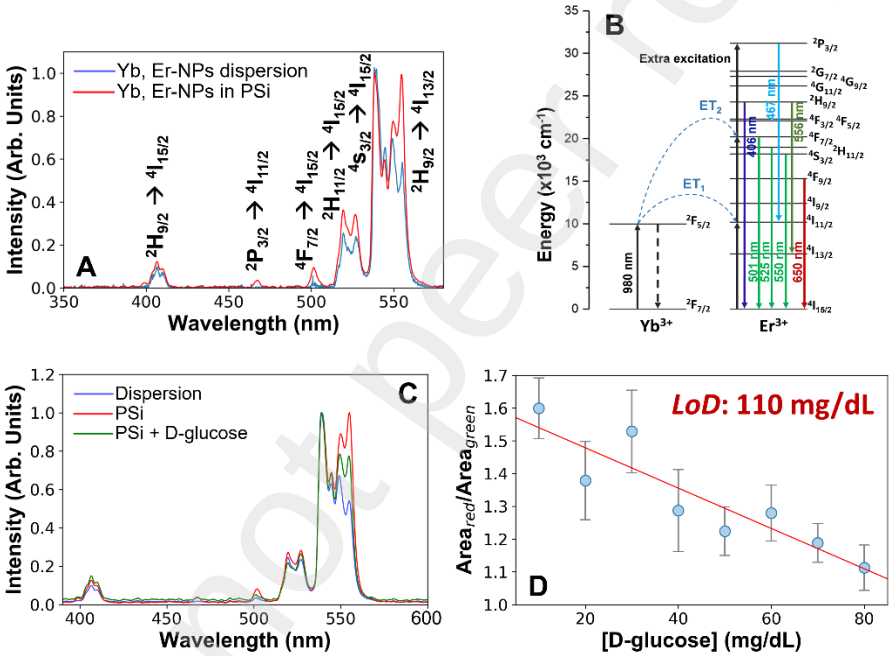

Figure 5. A. Extended up-conversion emission spectrum of YbEr-NPs in dispersion (10 mg/mL) and in PSi substrate. B**.** Energy-level diagram showing the transitions that appear in A. **C.** Comparison of the up-conversion emission spectra of YbEr-NPs in PSi (with and without D-glucose) with the same YbEr-NPs in the dispersion. **D.** New calibration curve representing the relationship between the 556/540 nm ratio and D-glucose concentration.

4. Conclusion

In this study, a porous silicon-based enzyme-free dual sensor was fabricated for future applications in noninvasive D-glucose detection through tear fluid analysis. Two electrodes were fabricated on top of the PSi substrate, allowing us to perform voltammetric analysis, which led to the first detection method using our sensor with a *LoD* of 20 mg/dL. This result offers an excellent range of detection because it is in the range of D-glucose concentrations in the tear fluids of patients with diabetes. In contrast, the YbEr-NPs on the surface of the detector provided a second detection method based on the changes in the up-conversion emission of the NPs after the interaction of the OH groups present in D-glucose with the Er^{3+}

ions in the NPs. The analysis of the red-to-green ratio for different concentrations of D-glucose allowed us to reach a *LoD* of 140 mg/dL, which is in the hyperglycemia range. The interaction between the YbEr-NPs and PSi provided a new source of excitation owing to the surface defects on the substrate, allowing it to reach higher energy levels of the Er^{3+} ions, producing an increase in the intensity of the 556 nm emission band, among others. This particular band was noticeably dependent on the concentration of D-glucose, allowing us to improve the *LoD* of our sensor to 110 mg/dL. This is a remarkable result that provides a novel strategy for D-glucose detection based on the effect of the molecule on the interaction between the UCNPs and the Psi substrate.

The results presented in this work provide a path for future noninvasive D-glucose detection in diabetic patients through tear fluid analysis, offering a way to measure concentrations in the hypoglycemic range through voltammetric analysis and in the hyperglycemic range through luminescence analysis of substrate-NP interactions.

Funding

This work was financed by the Comunidad de Madrid and Universidad Autónoma de Madrid (Project SI3/PJI/2021-00211). Additional funding was received from grant PID2020-118878RB-I00 (RETINanoTHERMIA) by MCIN/AEI/10.13039/501100011033; grant CNS2023-145366 funded by MICIU/AEI /10.13039/501100011033 and by the European Union NextGenerationEU/PRTR; grant PID2023-151371OB-C22 by MCIN/AEI/10.13039/501100011033 and by FEDER, EU; and grant CPP2021-008902 funded by MCIN/AEI/ 10.13039/501100011033 and by the "European Union NextGenerationEU/PRTR. Additional financial support from grant PID2020-116712RBC21 funded by MCIN/AEI/10.13039/501100011033 is acknowledged by A. A., and MICIN (Grant PID2020-113059GB-C22) is acknowledged by M.R.

References

[1] International Diabetes Federation, IDF Diabetes Atlas 2021 10th edition, (2021).
[2] D. Bruen, C. Delaney, L. Florea, D. Diamond, Glucose sensing for diabetes monitoring: Recent developments, Sensors (Switzerland) 17 (2017). https://doi.org/10.3390/s17081866.
[3] I. Conget, P UESTA AL D ÍA Diabetes y enfermedades cardiovasculares (I) Diagnóstico, clasificación y patogenia de la diabetes mellitus Sección patrocinada por el Laboratorio Dr. Esteve, 2002.
[4] P.E. Cryer, Hypoglycemia, functional brain failure, and brain death, Journal of Clinical Investigation 117 (2007). https://doi.org/10.1172/JCI31669.
[5] D. Giugliano, A. Ceriello, K. Esposito, Glucose metabolism and hyperglycemia, in: American Journal of Clinical Nutrition, 2008. https://doi.org/10.1093/ajcn/87.1.217s.
[6] Santiago Campillo, Hiperglucemia e hipoglucemia: causas, síntomas y tratamiento, (2022). https://www.vitonica.com/enfermedades/hiperglucemia-e-hipoglucemia-causas-sintomas-tratamiento (accessed February 13, 2023).
[7] Mayo Clinic, Hipoglucemia diabética - Síntomas y causas, (2022). https://www.mayoclinic.org/es-es/diseases-conditions/diabetic-hypoglycemia/symptoms-causes/syc-20371525 (accessed February 13, 2023).

[8] J.T. Baca, D.N. Finegold, S.A. Asher, Tear glucose analysis for the noninvasive detection and monitoring of diabetes mellitus, Ocular Surface 5 (2007). https://doi.org/10.1016/S1542-0124(12)70094-0.
[9] J.D. Lane, D.M. Krumholz, R.A. Sack, C. Morris, Tear glucose dynamics in diabetes mellitus, Current Eye Research 31 (2006). https://doi.org/10.1080/02713680600976552.
[10] J. T, S. R, R. J, A. Poojha, Novel Approach to Non-Invasive Blood Glucose Monitoring Based on Visible Laser Light, in: 2022 International Conference on Automation, Computing and Renewable Systems (ICACRS), 2022: pp. 54–57. https://doi.org/10.1109/ICACRS55517.2022.10029239.
[11] K.V. Larin, M.S. Eledrisi, M. Motamedi, R.O. Esenaliev, Noninvasive blood glucose monitoring with optical coherence tomography: A pilot study in human subjects, Diabetes Care 25 (2002). https://doi.org/10.2337/diacare.25.12.2263.
[12] T. Miura, A. Seiyama, M. Cassim, J. Seki, Improved Accuracy of Tissue Glucose Measurement Using Low Magnification Optical Coherence Tomography, IEEE Sensors Letters 5 (2021) 1–4. https://doi.org/10.1109/LSENS.2021.3126431.
[13] I. Ahmed, N. Jiang, X. Shao, M. Elsherif, F. Alam, A. Salih, H. Butt, A. K. Yetisen, Recent advances in optical sensors for continuous glucose monitoring, Sensors & Diagnostics 1 (2022) 1098–1125. https://doi.org/10.1039/D1SD00030F.
[14] K. Aslan, J.R. Lakowicz, C.D. Geddes, Nanogold-plasmon-resonance-based glucose sensing, Analytical Biochemistry 330 (2004). https://doi.org/10.1016/j.ab.2004.03.032.
[15] N. Mudgal, A. Saharia, A. Agarwal, J. Ali, P. Yupapin, G. Singh, Modeling of highly sensitive surface plasmon resonance (SPR) sensor for urine glucose detection, Opt Quant Electron 52 (2020) 307. https://doi.org/10.1007/s11082-020-02427-0.
[16] B. Karki, A. Jha, A. Pal, V. Srivastava, Sensitivity enhancement of refractive index-based surface plasmon resonance sensor for glucose detection, Opt Quant Electron 54 (2022) 595. https://doi.org/10.1007/s11082-022-04004-z.
[17] S.F. Malin, T.L. Ruchti, T.B. Blank, S.N. Thennadil, S.L. Monfre, Noninvasive prediction of glucose by near-infrared diffuse reflectance spectroscopy, in: Clinical Chemistry, 1999. https://doi.org/10.1093/clinchem/45.9.1651.
[18] K.E. Shafer-Peltier, C.L. Haynes, M.R. Glucksberg, R.P. Van Duyne, Towards a glucose biosensor based on surface-enhanced Raman scattering, Journal of the American Chemical Society 125 (2003). https://doi.org/10.1021/ja028255v.
[19] X. Sun, Glucose detection through surface-enhanced Raman spectroscopy: A review, Analytica Chimica Acta 1206 (2022) 339226. https://doi.org/10.1016/j.aca.2021.339226.
[20] J.W. Kang, Y.S. Park, H. Chang, W. Lee, S.P. Singh, W. Choi, L.H. Galindo, R.R. Dasari, S.H. Nam, J. Park, P.T.C. So, Direct observation of glucose fingerprint using in vivo Raman spectroscopy, Science Advances 6 (2020) eaay5206. https://doi.org/10.1126/sciadv.aay5206.
[21] H.A. MacKenzie, H.S. Ashton, S. Spiers, Y. Shen, S.S. Freeborn, J. Hannigan, J. Lindberg, P. Rae, Advances in photoacoustic noninvasive glucose testing, in: Clinical Chemistry, 1999. https://doi.org/10.1093/clinchem/45.9.1587.
[22] J.C. Pickup, F. Hussain, N.D. Evans, N. Sachedina, In vivo glucose monitoring: The clinical reality and the promise, in: Biosensors and Bioelectronics, 2005. https://doi.org/10.1016/j.bios.2004.08.016.
[23] Y. Cui, W. Duan, Y. Jin, F. Wo, F. Xi, J. Wu, Ratiometric Fluorescent Nanohybrid for Noninvasive and Visual Monitoring of Sweat Glucose, ACS Sens. 5 (2020) 2096–2105. https://doi.org/10.1021/acssensors.0c00718.
[24] T.V. Tam, S.H. Hur, J.S. Chung, W.M. Choi, Novel paper- and fiber optic-based fluorescent sensor for glucose detection using aniline-functionalized graphene quantum dots, Sensors and Actuators B: Chemical 329 (2021) 129250. https://doi.org/10.1016/j.snb.2020.129250.

[25] B. Viswanath, C.S. Choi, K. Lee, S. Kim, Recent trends in the development of diagnostic tools for diabetes mellitus using patient saliva, TrAC Trends in Analytical Chemistry 89 (2017) 60–67. https://doi.org/10.1016/j.trac.2017.01.011.
[26] R. Agrawal, V. Agarwal, Noninvasive Method for Glucose Level Estimation by Saliva, Journal of Diabetes & Metabolism 04 (2013). https://doi.org/10.4172/2155-6156.1000266.
[27] D.C. Caixeta, E.M.G. Aguiar, L. Cardoso-Sousa, L.M.D. Coelho, S.W. Oliveira, F.S. Espindola, L. Raniero, K.T.B. Crosara, M.J. Baker, W.L. Siqueira, R. Sabino-Silva, Salivary molecular spectroscopy: A sustainable, rapid and non-invasive monitoring tool for diabetes mellitus during insulin treatment, PLOS ONE 15 (2020) e0223461. https://doi.org/10.1371/journal.pone.0223461.
[28] H. Manoharan, D. J, S. A, An Intelligent Non-Invasive Sweat-Based Glucose Monitoring System for Managing Diabetes Mellitus, International Journal of Intelligent Systems and Applications in Engineering 12 (2024) 723–736.
[29] J. Xu, Y. Fang, J. Chen, Wearable Biosensors for Non-Invasive Sweat Diagnostics, Biosensors 11 (2021) 245. https://doi.org/10.3390/bios11080245.
[30] H. Zafar, A. Channa, V. Jeoti, G.M. Stojanović, Comprehensive Review on Wearable Sweat-Glucose Sensors for Continuous Glucose Monitoring, Sensors 22 (2022) 638. https://doi.org/10.3390/s22020638.
[31] S. Esfahani, A. Wicaksono, E. Mozdiak, R.P. Arasaradnam, J.A. Covington, Non-Invasive Diagnosis of Diabetes by Volatile Organic Compounds in Urine Using FAIMS and Fox4000 Electronic Nose, Biosensors 8 (2018) 121. https://doi.org/10.3390/bios8040121.
[32] M. Takakado, Y. Takata, F. Yamagata, M. Yaguchi, G. Hiasa, S. Sato, J. Funada, S. Kawazu, H. Osawa, Simple and non-invasive screening method for diabetes based on myoinositol levels in urine samples collected at home, BMJ Open Diabetes Res Care 8 (2020) e000984. https://doi.org/10.1136/bmjdrc-2019-000984.
[33] J.P. Bantle, W. Thomas, Glucose measurement in patients with diabetes mellitus with dermal interstitial fluid, Journal of Laboratory and Clinical Medicine 130 (1997) 436–441. https://doi.org/10.1016/S0022-2143(97)90044-5.
[34] E. De la Paz, A. Barfidokht, S. Rios, C. Brown, E. Chao, J. Wang, Extended Noninvasive Glucose Monitoring in the Interstitial Fluid Using an Epidermal Biosensing Patch, Anal. Chem. 93 (2021) 12767–12775. https://doi.org/10.1021/acs.analchem.1c02887.
[35] P.M. Wang, M. Cornwell, M.R. Prausnitz, Minimally Invasive Extraction of Dermal Interstitial Fluid for Glucose Monitoring Using Microneedles, Diabetes Technology & Therapeutics 7 (2005) 131–141. https://doi.org/10.1089/dia.2005.7.131.
[36] G. Glinská, K. Krajčíková, K. Zakutanská, O. Shylenko, D. Kondrakhova, N. Tomašovičová, V. Komanický, J. Mašlanková, V. Tomečková, Noninvasive diagnostic methods for diabetes mellitus from tear fluid, RSC Advances 9 (2019) 18050–18059. https://doi.org/10.1039/C9RA02078K.
[37] S.H. Lee, Y.C. Cho, Y. Bin Choy, Noninvasive Self-diagnostic Device for Tear Collection and Glucose Measurement, Sci Rep 9 (2019) 4747. https://doi.org/10.1038/s41598-019-41066-8.
[38] S.S. Adigal, A. Rizvi, N.V. Rayaroth, R.V. John, A. Barik, S. Bhandari, S.D. George, J. Lukose, Vasudevan.B. Kartha, S. Chidangil, Human tear fluid analysis for clinical applications: progress and prospects, Expert Review of Molecular Diagnostics 21 (2021) 767–787. https://doi.org/10.1080/14737159.2021.1941879.
[39] G. López-Peña, E. Ortiz-Mansilla, A. Arranz, N. Bogdan, M. Manso-Silván, E. Martín Rodríguez, Non-Invasive Paper-Based Sensors Containing Rare-Earth-Doped Nanoparticles for the Detection of D-Glucose, (2024). https://doi.org/10.2139/ssrn.4715804.

[40] P. Ravishankar, A. Daily, Tears as the Next Diagnostic Biofluid: A Comparative Study between Ocular Fluid and Blood, Applied Sciences 12 (2022) 2884. https://doi.org/10.3390/app12062884.
[41] A.C. Raposo, R.D. Portela, M. Aldrovani, T.D. Barral, D. Cury, A.P. Oriá, Comparative Analysis of Tear Composition in Humans, Domestic Mammals, Reptiles, and Birds, Frontiers in Veterinary Science 7 (2020). https://doi.org/10.3389/fvets.2020.00283.
[42] F. Bachhuber, A. Huss, M. Senel, H. Tumani, Diagnostic biomarkers in tear fluid: from sampling to preanalytical processing, Scientific Reports 11 (2021) 10064. https://doi.org/10.1038/s41598-021-89514-8.
[43] G. Kalló, M. Emri, Z. Varga, B. Ujhelyi, J. Tőzsér, A. Csutak, É. Csősz, Changes in the Chemical Barrier Composition of Tears in Alzheimer's Disease Reveal Potential Tear Diagnostic Biomarkers, PLOS ONE 11 (2016) e0158000. https://doi.org/10.1371/journal.pone.0158000.
[44] S. Hagan, E. Martin, A. Enríquez-de-Salamanca, Tear fluid biomarkers in ocular and systemic disease: potential use for predictive, preventive and personalised medicine, EPMA Journal 7 (2016) 15. https://doi.org/10.1186/s13167-016-0065-3.
[45] A. Barmada, S.A. Shippy, Tear analysis as the next routine body fluid test, Eye 34 (2020) 1731–1733. https://doi.org/10.1038/s41433-020-0930-0.
[46] T. Näreoja, T. Deguchi, S. Christ, R. Peltomaa, N. Prabhakar, E. Fazeli, N. Perälä, J.M. Rosenholm, R. Arppe, T. Soukka, M. Schäferling, Ratiometric Sensing and Imaging of Intracellular pH Using Polyethylenimine-Coated Photon Upconversion Nanoprobes, Analytical Chemistry 89 (2017) 1501–1508. https://doi.org/10.1021/acs.analchem.6b03223.
[47] M. Runowski, A. Shyichuk, A. Tymiński, T. Grzyb, V. Lavín, S. Lis, Multifunctional Optical Sensors for Nanomanometry and Nanothermometry: High-Pressure and High-Temperature Upconversion Luminescence of Lanthanide-Doped Phosphates—$LaPO_4$ /YPO_4:Yb^{3+}–Tm^{3+}, ACS Applied Materials & Interfaces 10 (2018) 17269–17279. https://doi.org/10.1021/acsami.8b02853.
[48] M. Runowski, P. Woźny, V. Lavín, S. Lis, Optical pressure nano-sensor based on lanthanide doped SrB2O4:Sm2+ luminescence – Novel high-pressure nanomanometer, Sensors and Actuators B: Chemical 273 (2018) 585–591. https://doi.org/10.1016/j.snb.2018.06.089.
[49] S. Shinoda, H. Miyake, H. Tsukube, Molecular recognition and sensing via rare earth complexes, in: Handbook on the Physics and Chemistry of Rare Earths, 2005. https://doi.org/10.1016/S0168-1273(05)35004-5.
[50] F. Vetrone, R. Naccache, A. Zamarrón, A. Juarranz de la Fuente, F. Sanz-Rodríguez, L. Martinez Maestro, E. Martín Rodriguez, D. Jaque, J. García Solé, J.A. Capobianco, Temperature Sensing Using Fluorescent Nanothermometers, ACS Nano 4 (2010) 3254–3258. https://doi.org/10.1021/nn100244a.
[51] D. Jaque, F. Vetrone, Luminescence nanothermometry, Nanoscale (2012). https://doi.org/10.1039/c2nr30764b.
[52] N. Bogdan, F. Vetrone, G.A. Ozin, J.A. Capobianco, Synthesis of Ligand-Free Colloidally Stable Water Dispersible Brightly Luminescent Lanthanide-Doped Upconverting Nanoparticles, Nano Letters 11 (2011) 835–840. https://doi.org/10.1021/nl1041929.
[53] M. Adeel, Md.M. Rahman, I. Caligiuri, V. Canzonieri, F. Rizzolio, S. Daniele, Recent advances of electrochemical and optical enzyme-free glucose sensors operating at physiological conditions, Biosensors and Bioelectronics 165 (2020) 112331. https://doi.org/10.1016/j.bios.2020.112331.
[54] Y. Bai, W. Yang, Y. Sun, C. Sun, Enzyme-free glucose sensor based on a three-dimensional gold film electrode, Sensors and Actuators B: Chemical 134 (2008) 471–476. https://doi.org/10.1016/j.snb.2008.05.028.

[55] G.P.C. Mello, E.F.C. Simões, D.M.A. Crista, J.M.M. Leitão, L. Pinto da Silva, J.C.G. Esteves da Silva, Glucose Sensing by Fluorescent Nanomaterials, Critical Reviews in Analytical Chemistry 49 (2019) 542–552. https://doi.org/10.1080/10408347.2019.1565984.
[56] J. Yuan, Y. Cen, X.-J. Kong, S. Wu, C.-L. Liu, R.-Q. Yu, X. Chu, MnO2-Nanosheet-Modified Upconversion Nanosystem for Sensitive Turn-On Fluorescence Detection of H2O2 and Glucose in Blood, ACS Appl Mater Interfaces 7 (2015) 10548–10555. https://doi.org/10.1021/acsami.5b02188.
[57] Y. Liu, D. Tu, W. Zheng, L. Lu, W. You, S. Zhou, P. Huang, R. Li, X. Chen, A strategy for accurate detection of glucose in human serum and whole blood based on an upconversion nanoparticles-polydopamine nanosystem, Nano Research 11 (2018) 3164–3174. https://doi.org/10.1007/s12274-017-1721-1.
[58] S. Wu, X.-J. Kong, Y. Cen, J. Yuan, R.-Q. Yu, X. Chu, Fabrication of a LRET-based upconverting hybrid nanocomposite for turn-on sensing of H2O2 and glucose, Nanoscale 8 (2016) 8939–8946. https://doi.org/10.1039/C6NR00470A.
[59] M. Wang, B. Lin, Y. Chen, H. Liu, Z. Ju, R. Lv, Fluorescence-Recovered Wearable Hydrogel Patch for In Vitro Detection of Glucose Based on Rare-Earth Nanoparticles, ACS Biomater. Sci. Eng. 10 (2024) 1128–1138. https://doi.org/10.1021/acsbiomaterials.3c01682.
[60] C. Zhang, Y. Yuan, S. Zhang, Y. Wang, Z. Liu, Biosensing platform based on fluorescence resonance energy transfer from upconverting nanocrystals to graphene oxide, Angew Chem Int Ed Engl 50 (2011) 6851–6854. https://doi.org/10.1002/anie.201100769.
[61] S. Dhanekar, S. Jain, Porous silicon biosensor: Current status, Biosensors and Bioelectronics 41 (2013). https://doi.org/10.1016/j.bios.2012.09.045.
[62] J. López-García, R.J. Martín-Palma, M. Manso, J.M. Martínez-Duart, Porous silicon based structures for the electrical biosensing of glucose, Sensors and Actuators, B: Chemical 126 (2007). https://doi.org/10.1016/j.snb.2006.10.050.
[63] I.S. Naiyeju, L.M. Bimbo, Chapter 5 - Biocompatibility of porous silicon, in: H.A. Santos (Ed.), Porous Silicon for Biomedical Applications (Second Edition), Woodhead Publishing, 2021: pp. 149–180. https://doi.org/10.1016/B978-0-12-821677-4.00014-8.
[64] C. Rodriguez, V. Torres-Costa, O. Ahumada, V. Cebrián, C. Gómez-Abad, A. Díaz, M. Manso Silván, Gold nanoparticle triggered dual optoplasmonic-impedimetric sensing of prostate-specific antigen on interdigitated porous silicon platforms, Sensors and Actuators B: Chemical 267 (2018) 559–564. https://doi.org/10.1016/j.snb.2018.03.179.
[65] N. Naveas, J. Hernandez-Montelongo, R. Pulido, V. Torres-Costa, R. Villanueva-Guerrero, J.P. García Ruiz, M. Manso-Silván, Fabrication and characterization of a chemically oxidized-nanostructured porous silicon based biosensor implementing orienting protein A, Colloids and Surfaces B: Biointerfaces (2014). https://doi.org/10.1016/j.colsurfb.2013.11.026.
[66] N. Naveas, V.T. Costa, D. Gallach, J. Hernandez-Montelongo, R.J.M. Palma, J.P. Garcia-Ruiz, M. Manso-Silván, Chemical stabilization of porous silicon for enhanced biofunctionalization with immunoglobulin, Science and Technology of Advanced Materials 13 (2012) 045009. https://doi.org/10.1088/1468-6996/13/4/045009.
[67] N. Naveas, M. Manso-Silván, E. Carmona, K. Garrido, J. Hernández-Montelongo, G. Recio-Sánchez, Green synthesized silver nanoparticles decorated on nanostructured porous silicon as an efficient platform for the removal of organic dye methylene blue, Green Chemistry Letters and Reviews 15 (2022) 108–115. https://doi.org/10.1080/17518253.2021.2024609.
[68] R. Williams, A.M. Goodman, Wetting of thin layers of SiO_2 by water, Applied Physics Letters 25 (1974) 531–532. https://doi.org/10.1063/1.1655297.
[69] J. Szade, M. Neumann, Exchange splitting of photoemission lines in GdF3 and metallic Gd compounds, J. Phys.: Condens. Matter 13 (2001) 2717. https://doi.org/10.1088/0953-8984/13/11/325.

[70] H. Fang, G. Kaur, B. Wang, Progress in boronic acid-based fluorescent glucose sensors, Journal of Fluorescence 14 (2004). https://doi.org/10.1023/B:JOFL.0000039336.51399.3b.
[71] Y. Cho, S.W. Song, S.Y. Lim, J.H. Kim, C.R. Park, H.M. Kim, Spectral evidence for multi-pathway contribution to the upconversion pathway in NaYF4:Yb3+,Er3+ phosphors, Phys. Chem. Chem. Phys. 19 (2017) 7326–7332. https://doi.org/10.1039/C7CP00048K.
[72] S.O. Ustalkov, E.A. Kozlova, O.A. Savenko, A.H.M. Mohammed, V.I. Kochubey, A.A. Skaptsov, Influence of excitation power density on temperature dependencies of NaYF4: Yb, Er nanoparticles luminescence spectra, in: Saratov Fall Meeting 2016: Optical Technologies in Biophysics and Medicine XVIII, SPIE, 2017: pp. 272–277. https://doi.org/10.1117/12.2269297.
[73] J. Kim, S.S. Joo, K.W. Lee, J.H. Kim, D.H. Shin, S. Kim, S.-H. Choi, Near-Ultraviolet-Sensitive Graphene/Porous Silicon Photodetectors, ACS Appl. Mater. Interfaces 6 (2014) 20880–20886. https://doi.org/10.1021/am5053812.
[74] S. Guha, P. Steiner, F. Kozlowski, W. Lang, Optical Characterization of Free-Standing Porous Silicon Films, Journal of Porous Materials 4 (1997) 227–237. https://doi.org/10.1023/A:1009623204014.